SIN-CHN
SCIENTIFIC PRESS PTE.LTD.

Molecular & Cellular Biomechanics 2025, 22(4), 876.
https://doi.org/10.62617/mcb876

Article

The role of CPAP therapy in modulating the biological mechanisms of hypertension and aortic aneurysm in obstructive sleep apnea patients

Yue Zhang, Wenfei Sun, Wenqian Wang, Feng Yu, Yixia Ai*

Jinan Metrology Verification and Testing Institute, Jinan 250014, China
*** Corresponding author:** Yixia Ai, aiyixia1106@163.com

CITATION

Zhang Y, Sun W, Wang W, et al. The role of CPAP therapy in modulating the biological mechanisms of hypertension and aortic aneurysm in obstructive sleep apnea patients. Molecular & Cellular Biomechanics. 2025; 22(4): 876. https://doi.org/10.62617/mcb876

ARTICLE INFO

Received: 22 November 2024
Accepted: 6 December 2024
Available online: 21 March 2025

Abstract: Background: Obstructive sleep apnea syndrome (OSAS) is closely related to multiple biological mechanisms, particularly its impact on the cardiovascular system. Long term OSAS may exacerbate issues such as hypertension, cardiovascular disease, and aortic disease. The aim of this study is to explore the effects of continuous positive airway pressure (CPAP) therapy on the biological mechanisms of OSAS patients, with a focus on analyzing the biological responses of blood pressure, respiration, and aortic changes. **Method:** This study retrospectively analyzed a case of a 75 year old male patient who was admitted with severe nighttime snoring and apnea symptoms, diagnosed with acute OSAS, aortic dissection, and hypertension. During the five-year follow-up after receiving CPAP treatment, the patient's apnea index (AHI), blood pressure, changes in aortic diameter, and related biological indicators were monitored. Comprehensive evaluation of treatment efficacy using multiple biomarkers and electrocardiogram (ECG) data, combined with optimization analysis of respiratory rate and electrocardiogram signals using electrophysiological models. **Result:** After five years of treatment, the patient's AHI significantly decreased to less than 6 beats per hour, blood pressure returned to normal, and the aortic diameter decreased from 4.5 cm to 4.1 cm. Electrophysiological analysis shows that CPAP treatment has a significant effect on adjusting respiratory patterns, restoring normal blood oxygen saturation, and optimizing the correlation between electrocardiogram and respiratory rate. In addition, using the TDNN model to estimate ECG signals shows a close biological correlation between respiratory rate and blood oxygen changes. **Conclusion:** CPAP treatment has a profound impact on the biological mechanisms of OSAS patients, effectively improving blood pressure control, reducing the progression of aortic disease, and optimizing changes in respiratory and electrocardiogram biomarkers. This study provides a new perspective for understanding the biological effects of OSAS treatment and provides a basis for optimizing future treatment strategies.

Keywords: electrocardiograph; ventilator calibration; internet of things; intelligent algorithms; deep learning; cloud platform; cardiovascular disease; real-time diagnosis

1. Introduction

Obstructive sleep apnea syndrome (OSAS) is a common sleep disorder characterized by repeated collapse of the upper airway during sleep, resulting in temporary respiratory pauses or inadequate ventilation [1,2]. With the incidence rate of OSAS increasing year by year, especially in obese and aging people, more and more studies have revealed its profound impact on overall health. OSAS not only affects sleep quality, but is also closely related to various pathophysiological mechanisms such as cardiovascular disease, metabolic disorders, and respiratory system diseases. In OSAS patients, the decrease in blood oxygen saturation caused by obstructive sleep apnea and long-term repeated hypoxic events can lead to biological reactions such as

increased sympathetic nerve activity, elevated blood pressure, and endothelial dysfunction, thereby exacerbating the development of cardiovascular disease. Especially for elderly patients, OSAS is often accompanied by serious complications such as aortic disease, which further exacerbates their condition [3,4].

In this context, continuous positive airway pressure (CPAP) therapy, as the gold standard method for treating OSAS, has been widely applied in clinical practice. CPAP effectively improves patients' sleep quality, reduces sympathetic nervous system activation, regulates blood pressure, and improves cardiovascular health by continuously maintaining upper airway patency, avoiding the occurrence of respiratory pauses and low oxygen events [5,6]. Multiple studies have shown that CPAP treatment can significantly reduce nighttime blood pressure in OSAS patients, reduce the occurrence of cardiovascular events, and effectively slow down the progression of vascular diseases such as the aorta. However, the profound effects of CPAP treatment on the biological mechanisms of OSAS patients have not been fully studied, especially its specific mechanisms of action on blood pressure regulation, electrocardiogram (ECG) signals, respiratory patterns, and progression of aortic disease [7,8].

In recent years, with the rapid development of biological technology, the analysis methods of biological signals such as electrocardiogram and sonocardiogram (PCG) have been continuously optimized, providing us with a new perspective for exploring the impact of OSAS on biological processes. Especially based on the analysis of electrocardiogram (ECG) signals, it can not only reveal the cardiovascular health status of patients, but also provide effective predictions for respiratory rate, blood oxygen changes, and other physiological processes [9,10]. The application of electrophysiological models, especially advanced technologies such as deep neural networks (TDNN), can effectively improve the estimation accuracy of electrocardiogram data and capture the complex correlations between respiration, heartbeat, and other biomarkers. Therefore, by combining modern biological techniques to conduct multidimensional evaluations of OSAS patients, we can comprehensively understand the profound impact of CPAP treatment on their biological mechanisms [11].

In this study, we selected a 75 year old male patient and evaluated the effects of CPAP treatment on blood pressure, aortic disease progression, respiratory patterns, and electrocardiogram signals based on clinical data and multiple biomarkers through a five-year follow-up of CPAP treatment. We paid special attention to the changes in important biological indicators such as blood pressure levels, apnea hypopnea index (AHI), and aortic diameter before and after CPAP treatment, and explored the role of CPAP treatment in improving these biological responses. By comprehensively analyzing the changes in ECG signals, respiratory rate, and aortic diameter, we aim to reveal the biological effects of OSAS treatment and explore the potential of CPAP therapy in improving patients' systemic physiological responses [12–14].

The goal of this study is to provide more targeted OSAS treatment strategies for clinical practice through scientific biological evaluation, and to provide theoretical basis for exploring the treatment mechanisms of related diseases in the future. The research results will help deepen our understanding of the biological mechanisms of OSAS and provide new ideas and methods for optimizing CPAP treatment plans,

delaying or reversing the progression of cardiovascular disease.

2. Analysis of demand

The word "quick" is emphasized while acquiring electrocardiograms for patients with cardiovascular disease. **Figure 1** illustrates the conventional ECG examination procedure. The patient's family members call 120 when they feel ill; the patient is taken to the hospital by ambulance; the receiving physician uses the ECG machine to identify and diagnose an abnormal ECG; the hospital opens the green channel for first aid, which typically takes between 15 and 26 min. This is a laborious and time-consuming process that takes an average of 26 min and at least 15 min. In order to improve the quality of emergency care for cardiovascular diseases in the area, it is necessary to set up an ECG monitoring and management system that incorporates a number of systems, including real-time ECG acquisition, display and storage, classification, diagnosis, early warning, and localization, into the platform architecture. This will enable quick, easy, and effective ECG diagnosis and early warning [15,16].

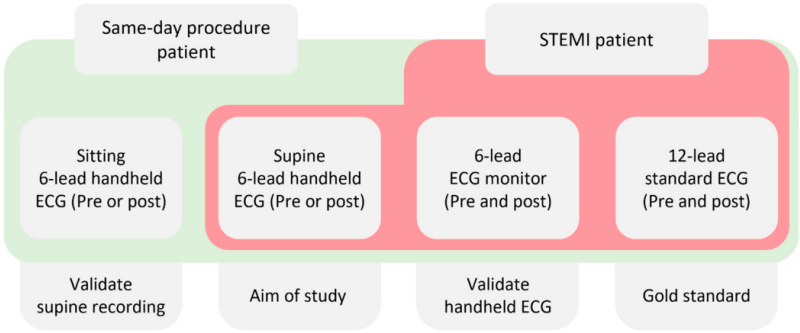

Figure 1. Standard ECG monitoring procedure.

3. Design of cloud platforms

3.1. Module for ECG acquisition

The ECG acquisition module, which combines a mobile application with an Internet of Things ECG machine, is in charge of data transmission, geographic location positioning, and the collection and processing of ECG signals. With a built-in AD8232 chip that converts the cardiac bioelectric signals recorded on the human skin into digital signals, the first generation of IoT ECG machines, the CAREDA-3, has achieved three-lead ECG acquisition. This is accomplished by three acquisition electrodes and one reference electrode. The ECG signal is a weak tiny signal that can be interfered with by baseline drift, industrial frequency interference, electromyographic noise, and other factors. The three acquisition electrodes are situated in the upper-left, upper-right, and lower-right positions of the chest, which correspond to the left arm, right leg, and right arm positions of the unipolar limb lead I, which makes up the right-leg drive amplifier. The purpose of the dedicated instrumentation amplifier is to amplify small signals and perform common-mode rejection. When the input current is applied, the common mode voltage change will be cancelled out, improving the system's common-mode rejection performance [16]. These guarantee that the IoT ECG equipment can efficiently extract weak ECG signals

while offering the highest level of noise suppression. Compared to traditional wet electrode measurement, the silver oxide dry electrode measurement used in the IoT ECG machine offers several benefits, including undistorted waveforms, high signal acquisition sensitivity, and the elimination of time-consuming procedures like applying conductive adhesive and conductive liquid [17]. Through low-power Bluetooth 4.0, the IoT ECG equipment is linked to the mobile application. Once the standard amount of time has been collected, the data can be transferred to the cloud platform or shown in real time. The data transmission function uses the Zigbee communication protocol, which has the qualities of low power consumption, low complexity, short latency, large capacity, and high reliability [18]. It involves uploading the ECG to the cloud platform via IoT for artificial intelligence diagnosis or sending it to the assigned physician for analysis. In order to help the cloud platform find cardiovascular patients and perform rescue treatment more effectively, the geolocation function transmits the patient's real-time position.

After turning on the ECG machine and successfully pairing the two devices via Bluetooth, the patient logs into the mobile application by entering their username and password. Register and fill up personal details like age and gender if this is the user's first time using it. After the ECG machine has stabilized its waveform, you can either hand it over to the doctor next to you for a direct reading or click on the capture of the effective length of time. Then, you can upload or send the ECG to the designated doctor by clicking on the upload button after waiting for the electrodes on the back of the machine to be recognized and automatically capture the ECG signals of the chest lead and display the real-time ECG signals on the APP on the cell phone terminal (see **Figure 2**).

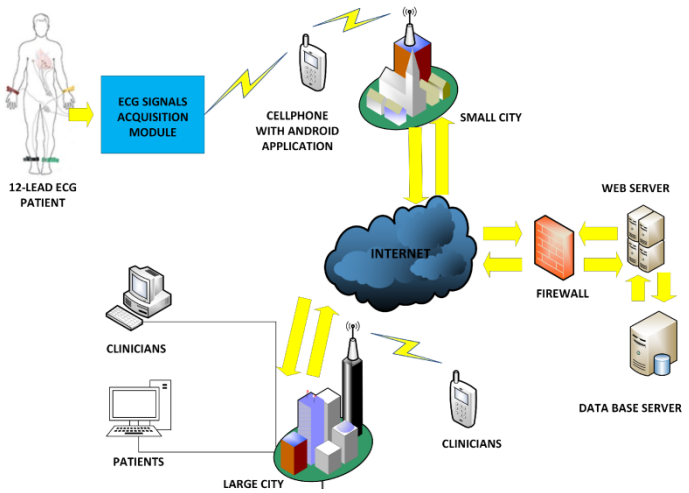

Figure 2. Diagram showing how the ECG capture module operates.

3.2. Algorithmic modules

Digital signals gathered by the ECG acquisition module are sent to the cloud platform's algorithm module, which uses artificial intelligence algorithms to categorize, identify, integrate, and analyze the ECG data before giving the user feedback. Filtering and baseline removal, feature point identification, QRS wave, atrial fibrillation, heart rate variability (HRV), R-wave classification, and rhythm type

analysis are the primary algorithms included in the algorithm module.

The baseline drift of ECG waveforms during routine ECG acquisition can be caused by breathing and position changes, as well as a variety of medium- and high-frequency electromagnetic induction interferences that can cause high waveform variability, feature obliteration and confusion, and unclear markers, all of which can complicate analysis [19]. In order to solve this issue, the algorithm module's filtering de-baseline algorithm computes the baseline drift value and eliminates baseline drift from ECG waveforms, making it simple to identify abnormal ECG waveforms [20]. Furthermore, the QRS wave algorithm was used to identify QRS wave clusters for RR interval and real-time heart rate calculation, while AF analysis was used to ascertain the start, stop, and duration of each occurrence of AF; HRV analysis algorithms can be used for both time-domain analysis (SDNN/SDSD/RMSSD/PNN50, etc.) and frequency-domain analysis (HF, LF, and UF, etc.); and the R-wave classification algorithm is used to identify normal rhythm, ventricular pre-systole, paired ventricular pre-systole, ventricular dysthymia, supraventricular ternary rhythm, arrest, atrial fibrillation, arrhythmia, tachycardia, and bradycardia. Fast analysis and precise diagnosis are guaranteed when the aforementioned algorithms run normally. **Figure 3** compares the ECG waveforms obtained simultaneously by four patients using this ECG machine and a 12-lead medical ECG machine, respectively. It also illustrates how the cloud platform processes ECGs and how aberrant waveforms are identified and labeled.

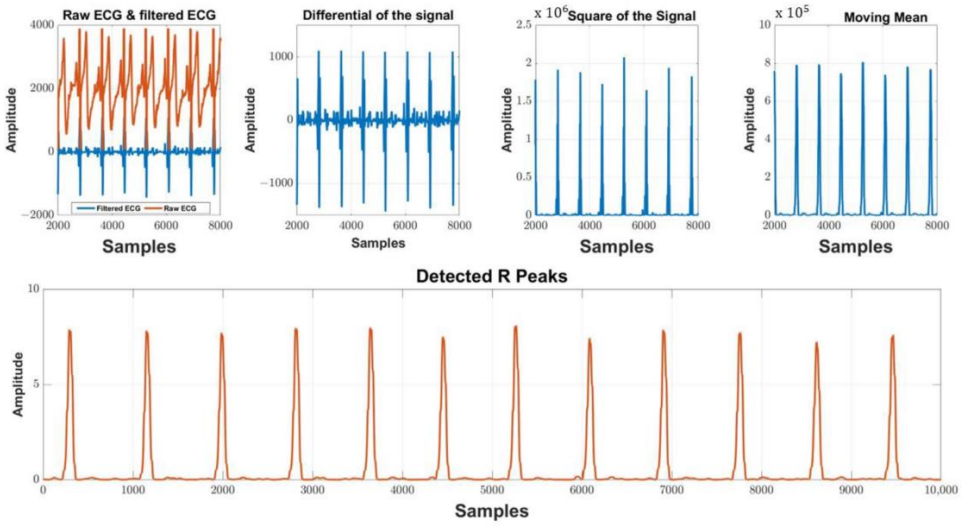

Figure 3. ECG waveforms recorded by medical and IoT ECG machines are compared.

3.3. Module for comparing diagnostic models

ECG data and algorithm analysis findings are stored in the diagnostic model comparison module for deep learning training and building illness diagnostic models.

Multiple diagnostic models are included in the module; these models are individually built using distinct techniques that carry diagnostic indicators. Deep learning is used to train these models using the ECG data samples that are kept in the module. The resulting deep predictions are then weighted to provide the final

integrated prediction. The deep learning model is chosen from a variety of machine learning Bayesian classifiers, K-nearest neighbor algorithm, K-mean algorithm, linear regression, logistic regression, multivariate nonlinear regression fitting methods, Adaboost algorithm, Hidden Markov Models, Extreme Learning Machines, Random Forests Algorithm, Decision Tree Algorithms, Generative Adversarial Networks, Stacked Auto-Encoders, Fully Connected Networks, Unsupervised Pretraining Networks, Deep Belief Networks, one or more deep Boltzmann machines, and neural tensor networks. Ultimately, multiple diagnostic models with various machine learning algorithms are obtained, and these are fused to create a comprehensive integrated model with a wide range of disease recognition capabilities for practical disease diagnosis. In fact, in the process of application, the back-end doctors of the cloud platform will also manually correct the AI diagnostic results, which is more advantageous in terms of accuracy and specificity compared to the pure AI diagnosis of Holter ambulatory electrocardiogram, which is to be followed up with a large-scale cross-sectional study for validation.

3.4. System of medical aid

The hospital has a medical aid system that includes the hospital chest pain center and the 120 emergency center. The doctor evaluates the diagnostic findings of the cardiovascular patient's ECG data supplied by the cloud platform and sends the judgment results back to the cloud platform after the cloud platform uses the Internet of Things to connect to the 120 emergency center or the chest pain center, sends the patient's ECG data, and provides the diagnostic results to the medical aid system. **Figure 4** displays the schematic of the cloud platform for IoT-based ECG machine ECG monitoring.

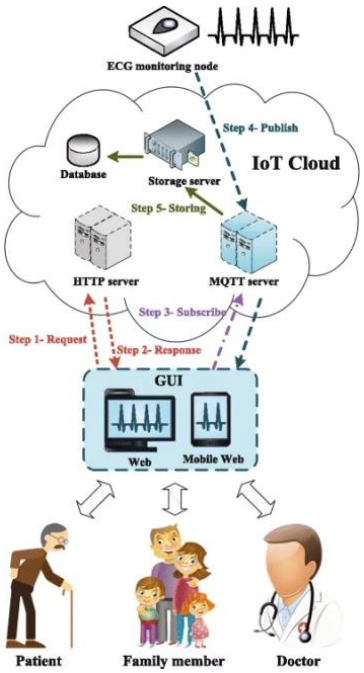

Figure 4. Cloud platform schematic for an Internet of Things-based ECG equipment for cardiac monitoring.

4. Result

4.1. Case

A 75-year-old male patient arrived at the clinic in September 2016 complaining of recurrent nighttime snoring that had been worsening for a month and had been going on for more than nine years. Past medical history: 4.5 cm in diameter ascending aortic aneurysm, found in April 2015 (refer to **Figure 5**); over ten years of hypertension; oral antihypertensive medicine; no history of smoking. Following his admission, he had polysomnography (PSG), which revealed a minimum oxygen saturation of 72% and an apnea hypopnea index (AHI) of 56.5 episodes per hour. He was diagnosed with a thoracic aortic aneurysm, hypertension, and acute OSAS when he was brought to the hospital. With a pressure of 8–10 cm H_2O and an average of 4.5 h, the patient was admitted to the hospital as part of a CPAP treatment program. After five years of follow-up, we discovered that the patient's sleep apnea had been successfully treated, that the AHI had decreased to six times per hour or less, that the blood pressure was within normal limits, and that the thoracic aortic aneurysm's diameter had not increased—in fact, it was beginning to shrink, as indicated in **Table 1**.

Table 1. Patient follow-up.

Index	Before treatment	Treatment for 5 years	Treatment for 8 years
AHI (times/h)	56.5	1.6	1.2
CPAP treatment pressure (cmH_2O)	10	7	7
Diameter of thoracic aortic aneurysm (cm)	4.5	4.4	4.1
BMI	22.8	24.5	23.2
LDL-C (mmol/L)	1.75	2.2	2.1
TC (mmol/L)	3.15	3.8	3.2
HbA1c (%)	5.5	5.8	5.2

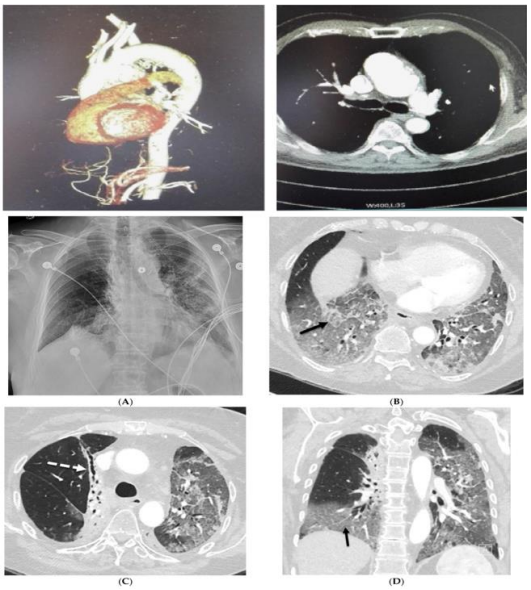

Figure 5. Enhancement of chest CT.

Note: 2016 chest CT enhancement: 4.5 cm thickening of the ascending aorta.

4.2. Estimation of electrocardiograms

The outcomes of the model selection phase for ECG lead estimate for ECG devices are displayed in **Figures 6a–c**. Only a portion of the TDNN results are displayed because the polynomial model and the MLP both perform noticeably worse than the TDNN. The best polynomial model has an order of magnitude of 9. Three layers with twelve neurons each make up the best MLP model. Models with the same lag parameter are indicated by the dashed lines in **Figure 6a**. It is evident that the BIC is much reduced as the maximum latency is increased. The BIC is slightly impacted by increasing the hidden layer's model complexity while maintaining a constant lag parameter. It is evident that a lag value of 70 to 80 is ideal when the average BIC for the highest model lag is provided in **Figure 6b**. The BIC curve's lowest point is shown in **Figure 6c**.

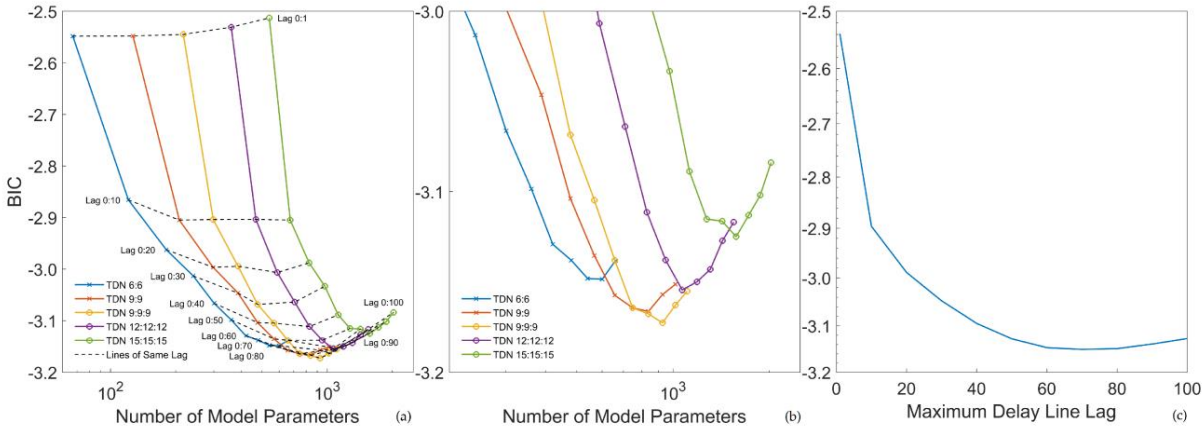

Figure 6. Choosing the BIC model for ECG lead estimate alone for TDNN: **(a)** choosing a line and model with a fixed lag length; **(b)** the lowest Bic value; **(c)** Bic on the quantity of lags in the delay line.

The average ECG estimate performance for the top model in each of the three model categories is shown in **Table 2** for all participants and locations. Generally speaking, the MLP's performance increase over the polynomial model is minimal. TDNN, on the other hand, greatly enhances performance.

The estimate for the second ECG lead, using the optimal TDNN model, revealed a linear correlation of 0.99 with a 5.5% relative error. With a linear correlation of 0.97 and a relative error of 1.6%, the correlation for the first ECG lead was marginally lower. There were no discernible variations in performance between the prone, lateral, and supine postures.

Table 2 shows the performance of the best polynomial, MLP, and TDNN models for patch ECG lead estimation for ECG I and II.

Table 2

Target ECG Lead	Model	$ME_{\mu}V$	$MAE_{\mu}V$	*r*	NMSE%
	Poly	0.01 ± 0.55	30.5 ± 10.5	0.66 ± 0.12	53 ± 25
Einthoven I	MLP	0.08 ± 0.05	28.6 ± 10.2	0.66 ± 0.15	50 ± 23
	TDNN	0.12 ± 0.55	9.6 ± 3.2	0.98 ± 0.02	5.6 ± 7.2
	Poly	0.22 ± 2.61	115 ± 48.5	0.77 ± 0.14	42 ± 23
Einthoven II	MLP	0.26 ± 3.4	110 ± 35	0.78 ± 0.15	40 ± 21
	TDNN	0.75 ± 1.22	23.5 ± 5.6	0.98 ± 0.01	1.6 ± 3.5

ECG excerpts from two distinct patients in the supine position simultaneously during the measuring procedure are displayed in **Figures 7** and **8**. The reference ECG leads and the estimated ECG signal are displayed in (b) and (c), whereas the 55-mm patch ECG is displayed in (a). The two persons' ECG leads are similar, however the patch ECG leads differ significantly. We noticed notable variations in the patch ECG leads' morphology across the participants during the course of the study. ECG leads may always be calculated for a certain performance, notwithstanding these variations.

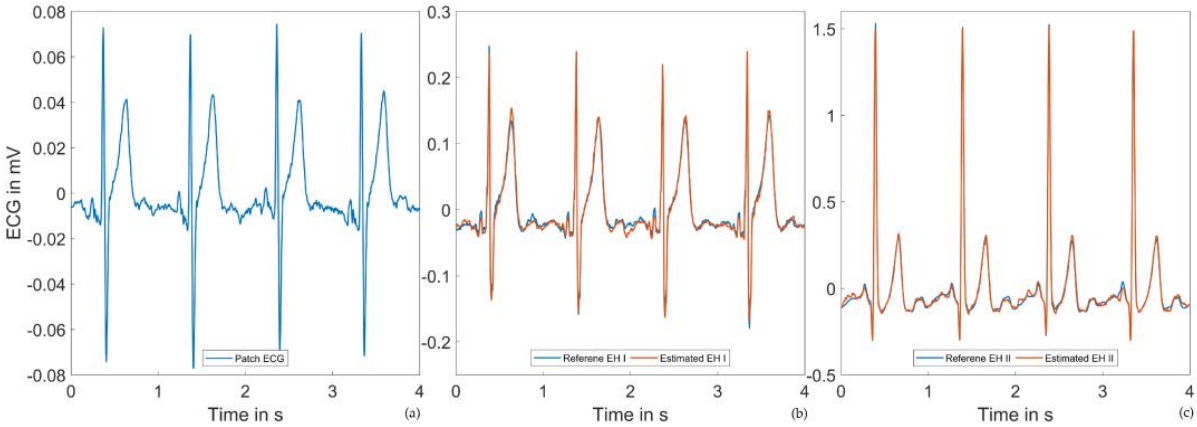

Figure 7. Example ECG readings for subject 1 while lying down: **(a)** patch ECG; **(b)** The estimated and reference ECG I ECG; **(c)** ECG II reference and estimated ECG.

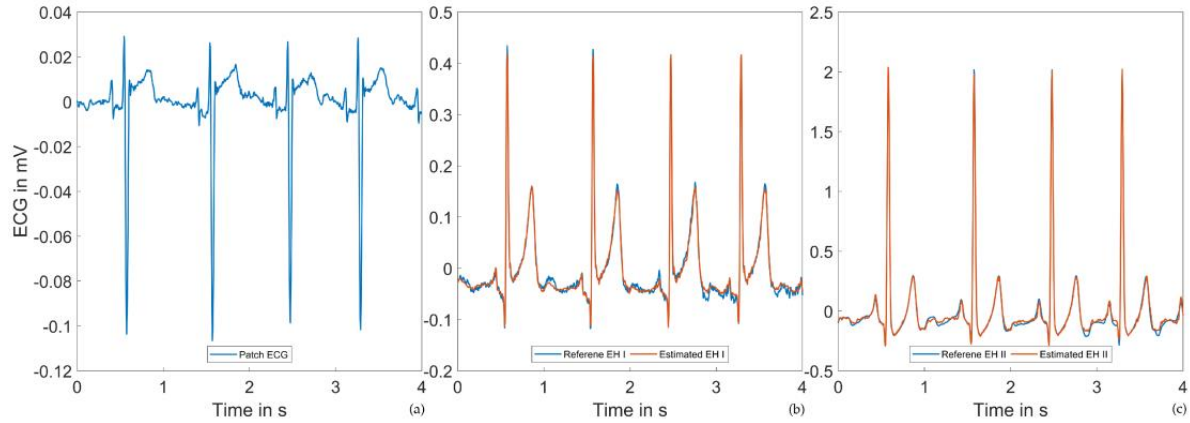

Figure 8. Examples of subject 2 supine ECG signals: **(a)** Patch ECG. In contrast to Figure 9a, a high degree of variability in the patch ECG leads across subjects can be observed; **(b)** Reference and estimated ECG I ECG; **(c)** Reference and estimated ECG II ECG.

4.3. Ventilator PEP and LVET estimates

An example of a ventilator ECG and PCG signal excerpt with the baseline point of detection within the simulated apnea period is shown in **Figure 9**. ECG peak detection worked successfully across all signals because of the good signal quality. Both the beginning and the peak of S1 and S2 were reliably identified in PCG. Because the end of S1 and the end of S2 were detected very early, the durations of the S1 and S2 peaks tended to be slightly underestimated.

The added noise caused by lung noises impairs PCG peak detection efficiency in low signal quality situations, particularly during the deep breathing period. The most frequent issue is false peak detection, which is hampered by the extra ECG data used during the classification stage. The suggested combined ECG and PCG peak detection approach detected two PCG peaks in 85.8% of the total stethoscope data. At 89.8%, the side-lying position performed the best, followed by the supine position (81.9%). 75.8% of the data were accessible for PCG peak detection when the subject was in the prone position.

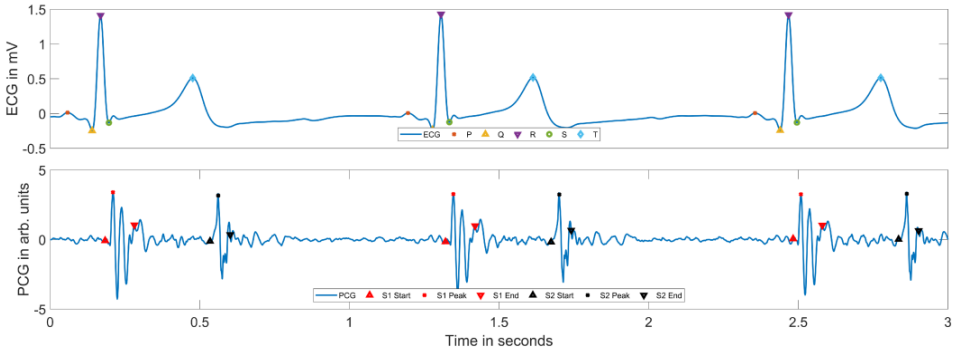

Figure 9. The reference point's ECG and PCG signals were detected.

Because the lateral recumbent position is similar to standard echocardiographic positioning, which has performance data published, **Table 3** presents the PEP and LVET estimation results. The PEP estimation error in this place was 15.6%. 7.0% was the relative LVET estimation error. However, additional places are of importance for dynamic estimation over the long period. We discovered that different sites had different LVET and PEP estimate performance. The PEP estimate was 25.1 ms for MAE and 0.4 ms for ME across all participants and locations, resulting in a relative error of 21.3%. With a relative error of 10.0%, the LVET estimates for ME and MAE were 3.6 ms and 30.5 ms, respectively.The PEP estimate was 25.1 ms for MAE and 0.4 ms for ME, resulting in a 21.3% relative inaccuracy.

Table 3. PEP and LVET estimates of ECG signals in the lateral position and aortic region auscultation.

Position	STI	ME_{ms}	MAE_{ms}	MAPE%
Lateral	PEP	6.15 ± 24.55	17.56 ± 15.86	16.02 ± 16.63
	LVET	−3.25 ± 32.56	21.82 ± 23.75	7.02 ± 7.26

Bland-Altman plots of STI estimates for PEP (a) and LVET (b) are displayed in

Figure 10. 302.2 ms is the average reference LVET, and 110.5 ms is the average reference PEP. The 5 ms resolution of the PEP and LVET references in ICON-Core is what causes the noticeable quantization. While the LVET plots typically include negative outliers that fall below 270 ms, the PEP plots display a sequence of positive outliers above 150 ms. Otherwise, the errors don't show any clear trends.

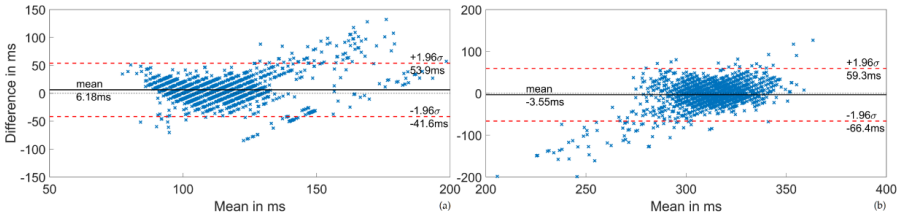

Figure 10. Bland-Altman plots of STI estimates: **(a)** PEP; **(b)** LVET.

4.4. Respiration derived from electrocardiograms and phonocardiograms

The correlation optimization model and feature selection of the predicted traffic signals are used to choose the TDNN with two hidden layers, two neurons per layer, and a tapped delay vector ranging from 0 to 9. r_{flow}, HR, QRS_{area}, $S1_{PCA}$ and QRS_{amp} are chosen from among the twelve EDR and PDR features that are accessible.

With a tap delay line latency of 0 to 14 and four neurons per layer, a two-layer TDNN functions optimally when the minimum MAE for the respiratory rate estimation MAE_{bpm} is optimized, and the HR, QRS_{area}, $S1_{PCA}$ and QRS_{amp} feature is chosen. The respiratory signal and rate estimate performance in relation to the flow reference is provided in **Tables 4** and **5**. Outliers have been eliminated from the data for each site, and data for the two optimization criteria are displayed separately. If a data point deviated more from the median than the absolute deviation from the three scaled medians, it was deemed an outlier.

Table 4 shows the performance of respiratory signal and rate estimate for every place in the optimization of maximum flow feature selection. It provides the percentage of outliers eliminated.

Table 4

Position	r_{flow}	ME_{bpm}	MAE_{bpm}	r_{RR}	**MAPE%**	**Outliers%**
Supine	0.74 ± 0.08	−0.01 ± 0.22	0.15 ± 0.14	0.90 ± 0.06	1.45 ± 1.42	9.50
Lateral	0.65 ± 0.12	−0.04 ± 0.32	0.22 ± 0.21	0.86 ± 0.02	1.88 ± 1.92	15.46
Prone	0.52 ± 0.12	0.05 ± 0.52	0.36 ± 0.38	0.78 ± 0.12	3.32 ± 3.87	22.75
All	0.680 ± 0.15	−0.02 ± 0.28	0.23 ± 0.18	0.88 ± 0.18	1.85 ± 1.99	15.6

Table 5 shows the performance of respiratory signal and rate estimate for every site in the feature selection optimization for minimal MAE bpm. The percentage of outliers eliminated is displayed.

Table 5

Position	r_{flow}	ME_{bpm}	MAE_{bpm}	r_{RR}	MAPE%	Outliers%
Supine	0.72 ± 0.12	0.01 ± 0.24	0.22 ± 0.15	0.91 ± 0.06	1.65 ± 1.43	9.55
Lateral	0.64 ± 0.15	−0.06 ± 0.32	0.22 ± 0.23	0.85 ± 0.02	1.84 ± 1.94	14.68
Prone	0.45 ± 0.12	0.01 ± 0.52	0.35 ± 0.38	0.78 ± 0.12	3.15 ± 3.87	21.75
All	0.62 ± 0.14	−0.02 ± 0.25	0.24 ± 0.19	0.88 ± 0.09	2.15 ± 2.26	12.56

The RR estimate bias is nearly zero in both optimization approaches. The RR estimate error is somewhat reduced as a result of the matching optimization feature selection. The flow signal correlation was higher for the correlation-optimized feature set. The positional correlation performance of all parameter estimates was consistently shown to be best in the supine position, followed by the lateral and prone orientations. The flow correlation dropped from 0.75 to 0.51 and the relative inaccuracy between the prone and supine positions more than quadrupled. Furthermore, the position of the subject had a significant impact on the quantity of outliers. Once more, the fewest aberrant results were found while the subject was in the supine position [21,22].

The Bland-Altman plots for the respiratory frequency estimations are displayed in **Figure 11a,b**, with all positions of the two optimization goals included and without outliers eliminated. It became clear that the study protocol called for three distinct breathing frequencies. Outliers were more likely to occur at lower and higher respiration rates, but there was no obvious rate-dependent error dependence.

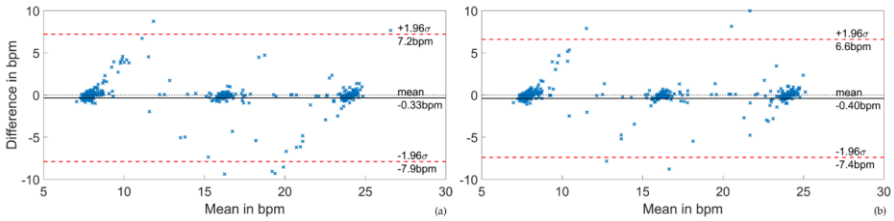

Figure 11. The performance plot of RR estimation using EDR and PDR at all places, including outliers: **(a)** optimization of correlation; **(b)** optimization of respiratory frequency.

A reference and calculated respiratory flow example for two distinct respiratory phases is shown in **Figure 12**. Over time, the estimated respiratory signal adjusts to the fluctuating breathing depth and follows the frequency. The piecewise nature of the underlying feature base makes it difficult to capture more detailed transitory patterns.

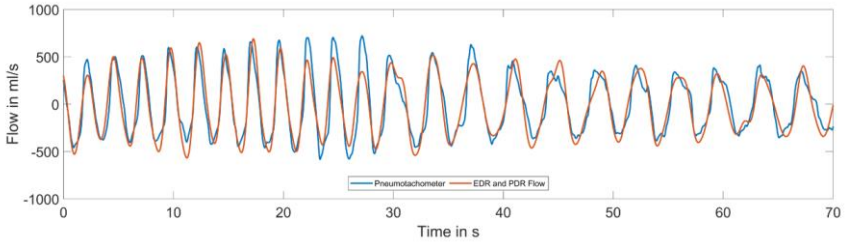

Figure 12. ECG and PCG-derived respiration examples of reference and estimated respiratory signals.

5. Conclusion

This study analyzed the biological effects of CPAP treatment on blood pressure regulation, aortic disease, electrocardiogram (ECG) signals, and respiratory patterns in a 75 year old male OSAS patient through a five-year follow-up of CPAP treatment. The research results indicate that CPAP treatment significantly improved the patient's apnea index (AHI), reducing it to less than 6 times per hour, and effectively controlled nighttime blood pressure levels, reducing the risk of cardiovascular events. At the same time, the patient's aortic diameter also showed a slight decreasing trend, indicating that CPAP treatment may have a positive effect on stabilizing aortic disease.

Through the analysis of electrocardiogram signals, especially the use of deep neural network (TDNN) models for ECG signal estimation, the study found that CPAP treatment not only improved ECG signals, but also optimized the synchronization between respiratory rate and heart rate, further confirming the positive impact of CPAP on the neural cardiovascular system interaction. By combining multidimensional data analysis of sound wave cardiac imaging (PCG) and ECG signals, we further revealed the mechanism by which CPAP therapy improves cardiovascular function at the biological level, particularly in reducing sympathetic nerve activity and decreasing cardiac burden.

In addition, this study also suggests that CPAP treatment not only has a direct effect on improving the sleep quality of OSAS patients, but may also have potential long-term health benefits by improving biomarkers and promoting the reversal of aortic lesions. This discovery provides a new biological perspective for the clinical treatment of OSAS in the future, and also provides a scientific basis for the long-term efficacy evaluation of CPAP therapy.

Conflict of interest: The authors declare no conflict of interest.

References

1. VITAZKOVA, Diana, et al. Advances in respiratory monitoring: a comprehensive review of wearable and remote technologies. Biosensors, 2024, 14.2: 90.
2. SUN, Zhigang, et al. Research on filtering and classification method for white-feather broiler sound signals based on sparse representation. Engineering Applications of Artificial Intelligence, 2024, 127: 107348.
3. LIU, Chang, et al. A review on the application of intelligent control strategies for post-stroke hand rehabilitation machines. Advances in Mechanical Engineering, 2023, 15.1: 16878132221148018.
4. Zhang, C., Xie, T., Yang, K., Ma, H., Xie, Y., Xu, Y., & Luo, P. (2019). Positioning optimisation based on particle quality prediction in wireless sensor networks. IET Networks, 8(2), 107-113.
5. BAIDILLAH, Marlin Ramadhan; BUSONO, Pratondo; RIYANTO, Riyanto. Mechanical ventilation intervention based on machine learning from vital signs monitoring: a scoping review. Measurement Science and Technology, 2023, 34.6: 062001.
6. WANG, Dong, et al. A supervised diagnostic experiment of resistance variable multifault locations in a mine ventilation system. Scientific Reports, 2023, 13.1: 5259.
7. LI, Zhihua, et al. A transformer-based deep learning algorithm to auto-record undocumented clinical one-lung ventilation events. In: International Workshop on Health Intelligence. Cham: Springer Nature Switzerland, 2023. p. 255-272.
8. CHEN, Dingfu, et al. An interpretable multi-scale lightweight network for patient-ventilator asynchrony detection during mechanical ventilation. Measurement, 2023, 222: 113597.
9. ANITHA, T.; GOPU, G.; ARUN MOZHI DEVAN, P. Mechanical Ventilator Pressure and Volume Control Using Classifier Machine Learning Algorithm for Medical Care. Journal of Electrical Engineering & Technology, 2024, 19.4: 2715-2738.
10. REN, Jianlin, et al. Experimental study on the physiological parameters of occupants under different temperatures and

prediction of their thermal comfort using machine learning algorithms. Journal of Building Engineering, 2024, 84: 108676.
11. VITAZKOVA, Diana, et al. Advances in respiratory monitoring: a comprehensive review of wearable and remote technologies. Biosensors, 2024, 14.2: 90.
12. SIVARANJANI, P., et al. IoT Based Smart Ventilator for Automatic Oxygen Flow. In: 2023 7th International Conference on Trends in Electronics and Informatics (ICOEI). IEEE, 2023. p. 463-471.
13. ZHANG, Gerui, et al. Research progress of respiratory disease and idiopathic pulmonary fibrosis based on artificial intelligence. Diagnostics, 2023, 13.3: 357.
14. VAN ES, Valerie AA, et al. Remote Monitoring of Sympathovagal Imbalance During Sleep and Its Implications in Cardiovascular Risk Assessment: A Systematic Review. Bioengineering, 2024, 11.10: 1045.
15. SHI, Rongzhen. Improvement of predictive control algorithm based on fuzzy fractional order PID. Journal of Intelligent Systems, 2023, 32.1: 20220288.
16. STASZAK, Katarzyna; TYLKOWSKI, Bartosz; STASZAK, Maciej. From data to diagnosis: How machine learning is changing heart health monitoring. International Journal of Environmental Research and Public Health, 2023, 20.5: 4605.
17. STASZAK, Katarzyna; TYLKOWSKI, Bartosz; STASZAK, Maciej. From data to diagnosis: How machine learning is changing heart health monitoring. International Journal of Environmental Research and Public Health, 2023, 20.5: 4605.
18. JENKINSON, Allan C.; DASSIOS, Theodore; GREENOUGH, Anne. Artificial intelligence in the NICU to predict extubation success in prematurely born infants. Journal of Perinatal Medicine, 2024, 52.2: 119-125.
19. Ibrahim, A., & Nazeer, S. On the Various Energy Forms of the Join of Complete Graphs. Journal of Combinatorial Mathematics and Combinatorial Computing, 122, 185-195.
20. SARKAR, Mekhla; LEE, Tsong-Hai; SAHOO, Prasan Kumar. Smart Healthcare: Exploring the Internet of Medical Things with Ambient Intelligence. Electronics, 2024, 13.12: 2309.
21. TIAN, Yuan, et al. Analysis of delirium prediction in the ICU based on the hybrid SGDCS-ANFIS approach. Medical & Biological Engineering & Computing, 2023, 61.3: 673-683.
22. WANG, Xiaokang, et al. Detection of outlying patterns from sparse and irregularly sampled electronic health records data. Engineering Applications of Artificial Intelligence, 2023, 126: 106788.